Research Article Vol. 12, No. 1 / 1 Jan 2022 / Optical Materials Express 272
Optical Materials EXPRESS

Check for updates

Room-temperature deposition of ZnS antireflection coatings for MIR-LWIR applications

Christian De Vita,[1,*] Marco Asa,[2] Claudio Somaschini,[2] Mikel Azpeitia Urquia,[3] Maria Eloisa Castagna,[4] Andrea Melloni,[1] and Francesco Morichetti[1]

[1] Dipartimento di Elettronica, Informazione e Bioingegneria (DEIB), Politecnico di Milano, Via Ponzio 34/5, Milano, Italy
[2] PoliFAB, Via Colombo 81, Milano, Italy
[3] STMicroelectronics, Via Camillo Olivetti 2, 20864 Agrate Brianza, Italy
[4] STMicroelectronics, Stradale Primosole 50, 95121 Catania, Italy
[*] christian.devita@polimi.it

Abstract: Integration of unconventional materials on established CMOS platforms requires to fulfill tight thermal budget constraints. However, low temperature processing may result in poor mechanical properties of the deposited films, which can exhibit stress-induced degradation of the optical properties or even delamination. This work focuses on a CMOS-compatible low-temperature deposition process for ZnS films on silicon and its use for the realization of an antireflection coating (ARC) operating in the medium infrared (MIR)–longwave infrared (LWIR) range. A thin interlayer of Al_2O_3 is employed to achieve good adhesion of a ZnS film deposited on Si by e-beam evaporation at room temperature. Numerical simulations are carried out to optimize the performance of single- and double-side ARC structures, quantifying the impact of the Al_2O_3 interlayer and of the fabrication tolerances on the optical transmission. Experimental results on an 8” silicon wafer demonstrate a peak transmittance of 66% for single-side ARC and 89% for a double-side ARC at a wavelength of 10 µm, resulting in an average transmission of 76.2% for black body radiation at 36 °C in the 6–20 µm wavelength range.

© 2021 Optical Society of America under the terms of the OSA Open Access Publishing Agreement

1. Introduction

Infrared wavelengths are crucial in many applications, such as communications, lasers, medical and bio sensing and night vision systems. Mid-wavelength infrared (3–8 µm) is well-known as the wavelength range characterizing most of the thermal emissions and absorption peaks related to environmental gasses [1]. Blackbody radiation at 300 K has its peak around 10 µm, making the Long Wavelength InfraRed (LWIR) band interesting for various civilian and military purposes, such as tracking and positioning. Silicon, which is the fundamental semiconductor in microelectronics, has nowadays gained a wide role also in photonics, where has been widely exploited in bulk and integrated devices. Considering its high refractive index (n_{Si}=3.418@10 µm) [2], silicon allows to reduce the dimensions of many photonic elements thanks to the possibility of realization of high index contrast structures. Yet, strong reflections could occur when interfaced with low index materials, up to 30% for the silicon-air interface, making necessary the use of an antireflection coating (ARC).

This paper proposes and demonstrates an ARC operating at 10 µm to reduce the reflections from the air-silicon interface in devices operating in free space. Ideally, a simple ARC can be implemented by depositing a quarter wavelength layer with refractive index $n_{ARC}=\sqrt{n_{air}n_{Si}}=1.86$ and thickness $d_{ARC}=\lambda/4n_{ARC}=1.34$ µm. Such a solution guarantees a reflectivity lower than 1% over a wavelength range of 1.4 µm. In addition to the optical requirements, however, the choice of

#439843 https://doi.org/10.1364/OME.439843
Journal © 2022 Received 6 Aug 2021; revised 27 Oct 2021; accepted 22 Nov 2021; published 22 Dec 2021

the material and the technological process are of main importance. Figure 1 reports a selection of materials with a good transparency in the LWIR and their refractive index at the wavelength of 10 µm. Even if materials such as CsI and KBr are more suitable from the optical point of view, ZnS exhibits a broad range of transparency from visible to far IR and a refractive index of 2.2 at 10 µm, these features making it appear as a good candidate for the realization of an ARC on silicon operating at infrared wavelength. ZnS is indeed already used in the infrared for the construction of lenses, windows or domes [3] and can be prepared by many deposition techniques such as thermal evaporation [4], chemical bath deposition [5], sputtering and others [6–8].

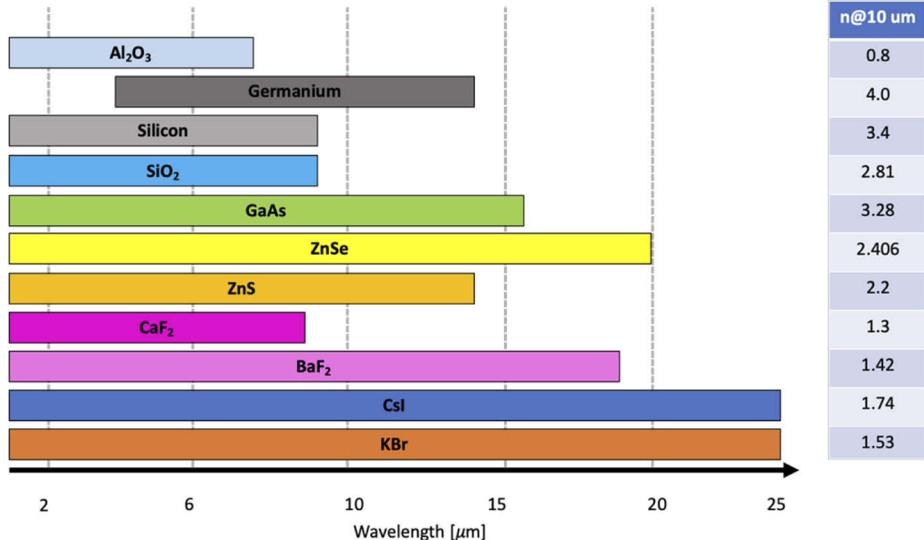

Fig. 1. Transparency region of materials for ARC applications with refractive index at @10 µm.

In literature, most ARCs for infrared are deposited at high temperatures [9–11]. More specifically realizing a low-temperature-process ARC on silicon operating in the 10 µm wavelength range is still an open issue. The aim of this work is to propose an ARC deposited at room temperature, making possible the use in back end on CMOS- or polymer- based silicon devices and allowing the use of standard photoresists for lift-off process. In Section 2 the deposition recipe and the film characterization are described. Section 3 presents the design of the ARC and the expected spectral characteristics are discussed. Section 4 is dedicated to the experimental validation of a single and double ARC deposited on a silicon wafer.

2. Film deposition and characterization

The ARC study has been conducted by using 8” Si <100> wafers, which are single or double side polished in case of ARC on one or two sides. The deposition of the ZnS films was performed by e-beam evaporation with an Evatec BAK 640 machine, which is able to handle up to six 8” wafers in a single run. The evaporation was performed at a pressure of 10^{-7} mbar from ZnS grains of 3–12 mm size with a purity of 99.99%. The deposition rate is 4 nm/s. Targeting a low temperature process, the effect of the deposition temperature on the film quality in term of optical properties, adhesion, film stress, etc. was investigated. Figure 2 shows the stress measured on 1-µm-thick ZnS films deposited for substrate temperatures from room temperature up to 250°C. Stress measurements were performed by KLA Tencor P-17 profilometer from the wafer curvature by using a Stoney model [12].

Optical Materials EXPRESS

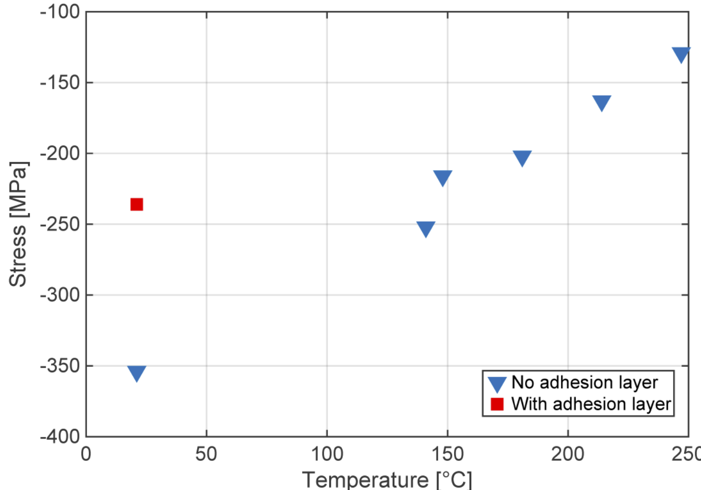

Fig. 2. Stress of e-beam evaporated ZnS films deposited on a Si substrate at increasing substrate temperatures. The red square refers to the result achieved with a 20-nm-thick intermediate Al_2O_3 adhesion layer.

Results show that decreasing the deposition temperature the compressive stress increases by almost a factor three, from −130 MPa to about −350 MPa. Above 200°C (compressive stress module >−200 MPa) the adhesion is excellent while with deposition at room temperature the ZnS film exhibits a very poor adhesion, not passing the MIL-F-48616 standard tape test [13], confirming the behavior observed in previous works [14]. Figure 3(a) shows the photo of a low-temperature processed wafer, exhibiting evident cracks due to the high stress and poor adhesion. The detail given in Fig. 3(b) demonstrates that even in the regions where no macroscopic cracks are visible, the film exhibits typical features due to film delamination.

A viable solution to improve the adhesion at low deposition temperature is the addition of a thin interlayer at the ZnS-Si interface. This strategy was successfully adopted in [15], where a thin MgO film is used for the low-temperature deposition of ZnS on a germanium (Ge <111>) substrate. In our process we employed a thin layer of Al_2O_3, whose thickness (20 nm) is the minimum thickness guaranteeing good adhesion of the ZnS film to the Si substrate and at the same time gives acceptable loss in the LWIR range (see Sec. 3). The Al_2O_3 layer was evaporated at room temperature prior to ZnS from grains of 1.5–4 mm with a purity of 99.99%. The Al_2O_3 layer reduces the stress from −350 MPa to less than −240 MPa (red square in Fig. 2) facilitating the good adhesion of the ZnS film over the entire wafer surface. The aspect of the film is shown in Fig. 3(c) and 3(d) where neither macroscopic fracturing nor delamination are visible in the wafer. The good adhesion of the ZnS film to the Si substrate is confirmed by standard MIL-F-48616 tape test followed by a scanning electron microscopy (SEM) analysis. Figure 4 shows the ZnS/Al_2O_3/Si layer stack cross-section demonstrating also the compactness of the ZnS all over the film cross section. The 20-nm-thick Al_2O_3 film is just perceivable due to the 10 nm resolution of our SEM. In this sample the total thickness of the entire coating stack, including the 20-nm-thick Al_2O_3 interlayer, is about 1120 nm, which is close to the target thickness of the ARC device designed in Sec. 3. The effects of the Al_2O_3 layer (d_{Al2O3}) on the optical performance of the ARC will be presented further.

To assess the optical properties of the ZnS film, the refractive index n and the extinction coefficient k were measured in the wavelength range from the visible (400 nm) to the near-IR (1650 nm) by using spectroscopic ellipsometry (Woolam V.A.S.E. Ellipsometer). Figure 5(a) shows the dispersion curves for the room-temperature ZnS layer deposited on top of Al_2O_3/Si

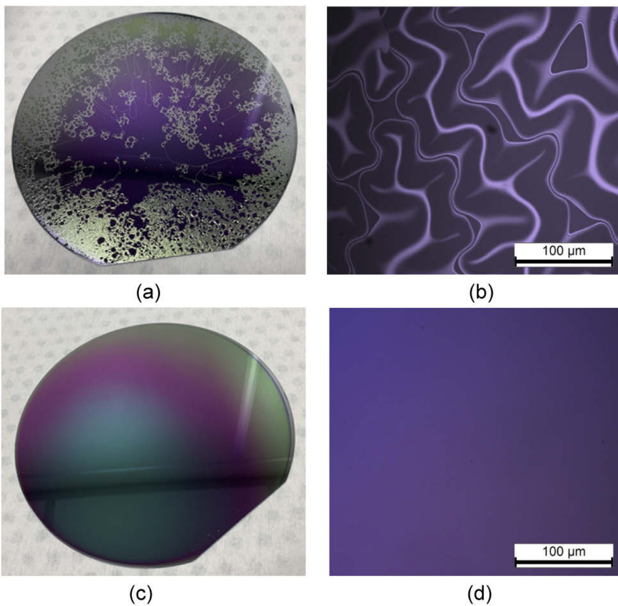

Fig. 3. Room-temperature ZnS e-beam evaporation on an 8” silicon wafer: (a) direct ZnS deposition (no adhesion interlayer) results in macroscopic cracking and (b) local delamination effects. The addition of a 20-nm-thick Al_2O_3 interlayer between the ZnS film and the Si substrate results in improved adhesion and no cracking as shown in the macroscopic (c) and microscopic (d) wafer inspection. Details (b) and (d) refers to the central part of the wafers.

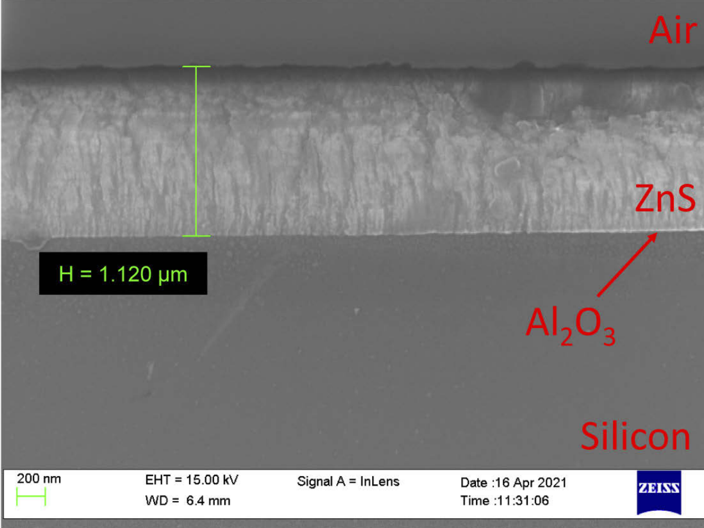

Fig. 4. SEM photo of the ARC cross section.

substrate. Prism coupling technique (Metricon 2010) confirms the value of the refractive index $n = 2.3474$ ($\pm$ 10^{-4}) at $\lambda = 633$ nm and $n = 2.265$ ($\pm$ 10^{-4}) at $\lambda = 1550$ nm, which are in line with results reported in the literature [16]. Figure 5 shows the ZnS thickness (b) and refractive index (c) measured in seven different points across the wafer. The uniformity of the film thickness and of the refractive index are $\pm$ 25 nm (around a target thickness of 1050 nm) and $\pm$ 2e-4 (around the

Optical Materials EXPRESS

reference refractive index at 633 nm), demonstrating the good quality of the deposition process across the 8” wafer. As shown in the following section, these tolerances are within the sensitivity constraints of the ARC targeted in this work.

To prove the quality of the adhesion layer with a low temperature deposition, a lift-off process was carried out on an 8” wafer with aluminum features previously patterned on it. After a careful cleaning of the substrate, MicroChemicals AZ nLof 2070 photoresist was spun and patterned

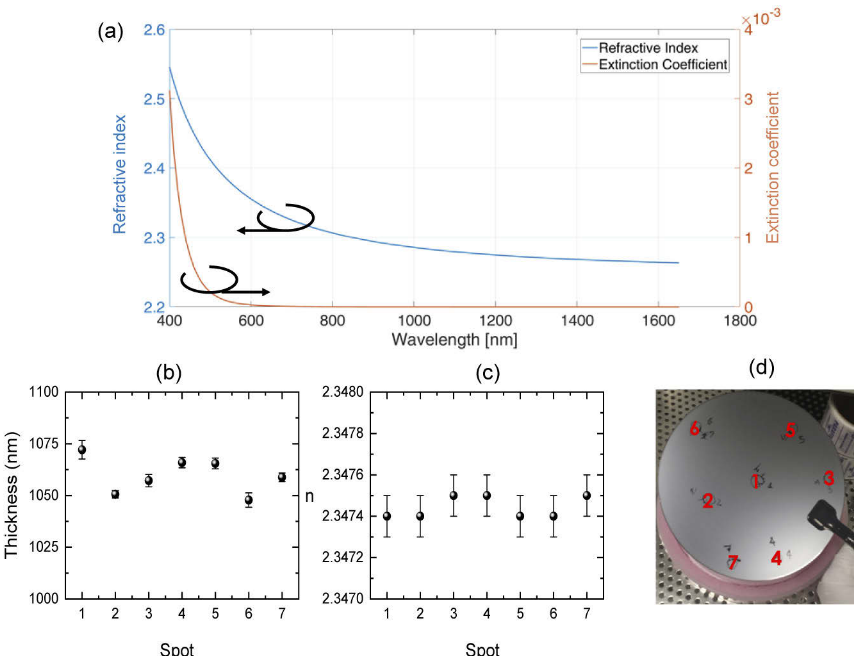

Fig. 5. (a) Refractive index n and extinction coefficient k of room-temperature deposited ZnS in the visible and near-IR wavelengths. Uniformity of thickness (b) and refractive index measured at 630 nm (c) on 7 spots of a ZnS layer with a nominal thickness of 1050 nm deposited on an 8” Si wafer (d).

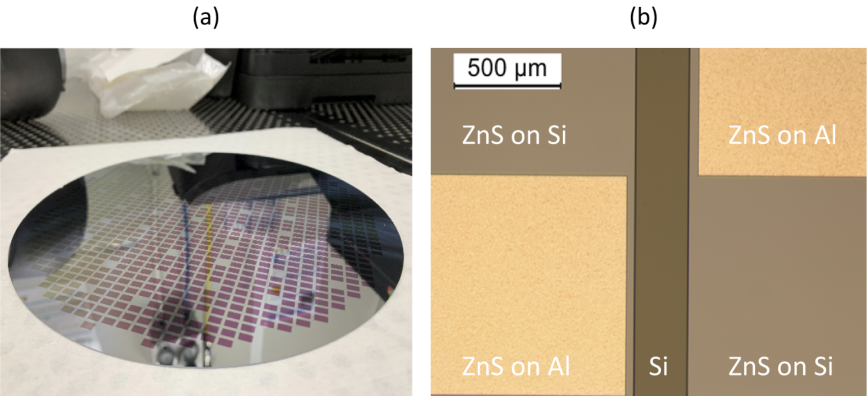

Fig. 6. (a) Photo of the lift-off patterned ARC on a 8” silicon wafer. (b) Detail of two features patterned with ZnS and separated by a trench. The brighter areas show where ZnS is deposited on top of aluminium features realized onto the silicon wafer.

Optical Materials EXPRESS

on the wafer, then the ARC stack was evaporated on it with the deposition process previously described, and finally the lift-off was carried out by DMSO bath. Figure 6(a) shows the full wafer with patterned ZnS regions after rinse and dry treatment, the features in this specific case being a few mm wide. Microscopic optical inspection in Fig. 6(b) shows that the ZnS features were well defined, with neither ZnS delamination nor traces of off-pattern residues, both in the regions where the ZnS is deposited on silicon and on aluminum.

3. ARC design

The quarter wavelength ARC in ZnS has been tested on a 700-μm-thick double-polished silicon wafer. Two structures have been considered, consisting of a ZnS film deposited on one side of the Si wafer and on both sides. Figure 7(a) and (b) show a schematic of the two structures, including the Al_2O_3 adhesion layer. The refractive index n and the extinction coefficient k of the different materials of the stack are reported in Figs. 7(c) and (d) over a large wavelength range. The dispersion curves of ZnS [17] and Al_2O_3 [18] are taken from literature, while for Si we extracted the material parameters from a transmission measurement performed by using a Fourier Transform Infrared Spectrometer (FTIR).

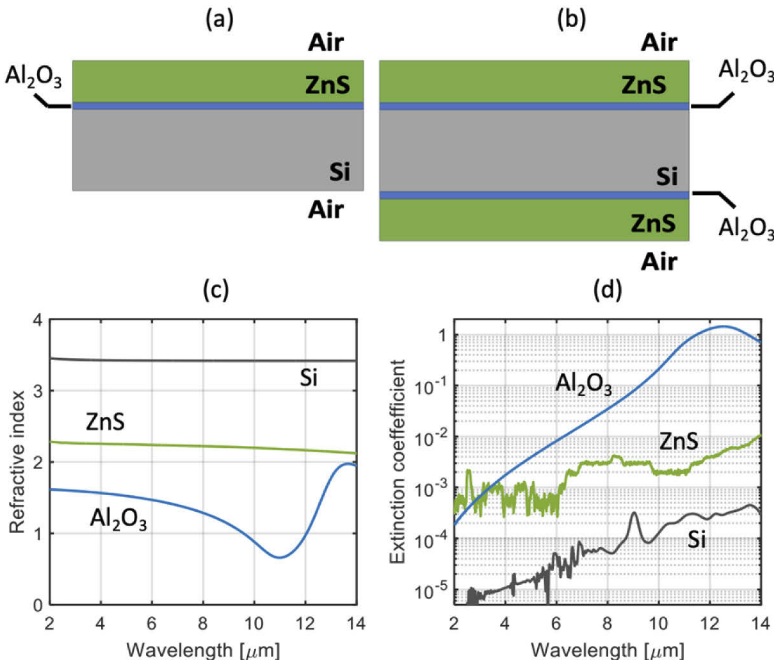

Fig. 7. Single ARC stack (a) and double ARC stack (b). Layer thicknesses are not in scale. (c) Refractive index n and (d) extinction coefficient k of Al_2O_3, ZnS and silicon in the MIR and LWIR.

Numerical simulations based on a transmission matrix method (TMM) [19] software tool were carried out in order to optimize the transmission performance of the ARC. Nominally, a quarter wavelength ARC for silicon should have the refractive index equal to 1.86. This ideal quarter wavelength ARC could reach up to 94.8% transmission with a double layer, keeping the reflectance below 1% over a wavelength range of 1.45 μm. However, as previously discussed, a material with such refractive index is not readily available in the LWIR and ZnS has been used as a best compromise between technological issues and optical properties. The refractive index n is 2.199 at $\lambda_0 = 10$ μm and hence the thickness has to be $d = \lambda_0 / 4n = 1.136$ μm.

Optical Materials EXPRESS

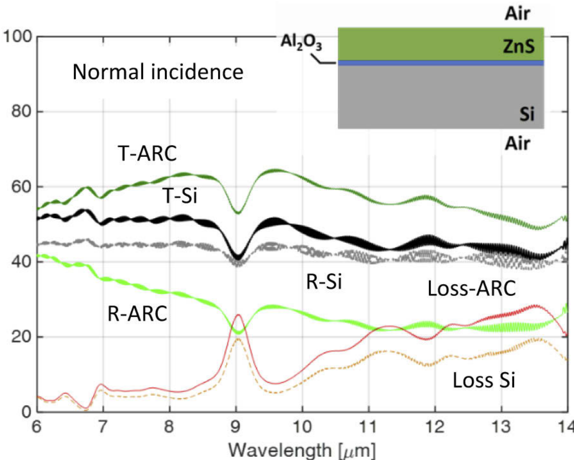

Fig. 8. Simulated Transmittance (T), Reflectance (R) and Loss of a 700 μm thick silicon wafer with single side ARC (shown in the inset) compared with an uncoated silicon wafer. The curves have been smoothed with a moving average filter of 0.15 μm.

In the simulations, the optical field impinging on the structure is assumed to be a plane wave with a given polarization state (*s* or *p*) and a variable orientation of the wave vector with respect to the normal to the ARC surface. Both considered structures are assumed in air. The analysis refers to the 6–14 μm wavelength range (while experimental results extend up to 20 μm), because above 14 μm no reliable data on the Al_2O_3 extinction coefficient are available in the literature.

Figure 8 shows the comparison between the wavelength dependent intensity transmission (T) and reflection (R) of the single side ARC (ZnS/Al_2O_3/Si) with respect to an uncoated Si wafer. Here, we assumed the nominal thicknesses d_0 for the ZnS layer, while for the Al_2O_3 layer a thickness of 20 nm is considered, as already explained in Sec. 2. A moving average filtering over a bandwidth of 0.15 μm is applied to all the curves in order to reduce the Fabry-Pérot oscillations and extract the mean value of the spectrum. Because of the increase of the Si absorption versus wavelength, the transmission of the uncoated Si film (T-Si, black line) drops from 54% at a wavelength of 6 μm to about 42% at 14 μm. The transmission notch at 9 μm is due the Si-O-Si molecular absorption of Czochralski grown Si where oxygen impurity levels can be in the order of 10^{18} cm^{-3} [20]. At the nominal central wavelength $\lambda_0 = 10$ μm, the ARC increases the maximum intensity transmission from 50% to 64% (T-ARC, green line), that is about 28% relative increase. The central wavelength of the transmission band occurs around 9 μm because of the absorption of both Si and Al_2O_3 films, amounting to less than 5% at 8 μm and more than 20% at 12 μm (Loss-ARC, red line) and 19% at 9 μm. The spectral band with more than 60% transmission is 3 μm wide, from 7.3 μm to 10.3 μm. Since the extinction coefficient *k* of the ZnS film is lower than 3e-3 in the 8–12 um wavelength range [see Fig. 7(b)], its contribution to the overall loss introduced by the ARC is almost negligible (<1%). The transmission improvement given by the ARC extends all across the considered wavelength range, vanishing only around 5 μm where the ZnS film behaves as a half-wavelength layer.

Figure 9 shows the comparison between the double side ARC (2ARC) structure (ZnS/Al_2O_3/Si/Al_2O_3/ZnS) and the uncoated Si wafer. The two ARCs are realized with the same thicknesses - 20 nm of Al_2O_3, 1.136 μm of ZnS - as in the single ARC case. The double side ARC improves the maximum transmittivity at the nominal central wavelength 10 μm from 50% to 83%, that is a relative increase by 66% and 29% with respect to the uncoated Si wafer and the single ARC, respectively. The presence of the ARC at the second interface reduces the reflection below 10% in the wavelength range 8.5–13.4 μm (R-2ARC, light green line) with a significant improvement

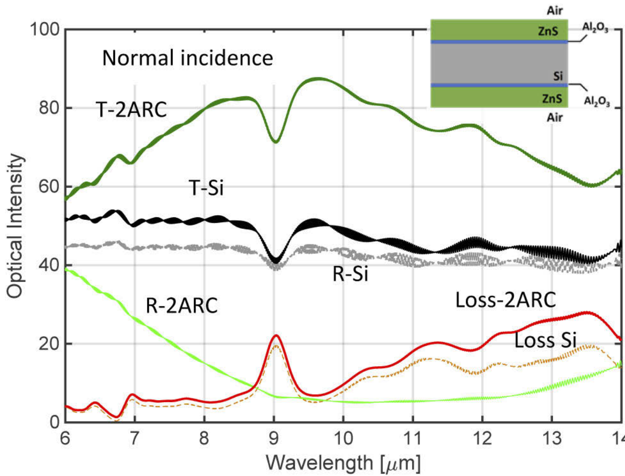

Fig. 9. Simulation of the Transmittance (T), Reflectance (R) and Loss of a 700 μm thick silicon wafer with double side ARC (shown in the inset) compared with an uncoated Si wafer. The curves have been smoothed with a moving average filter of 0.15 μm.

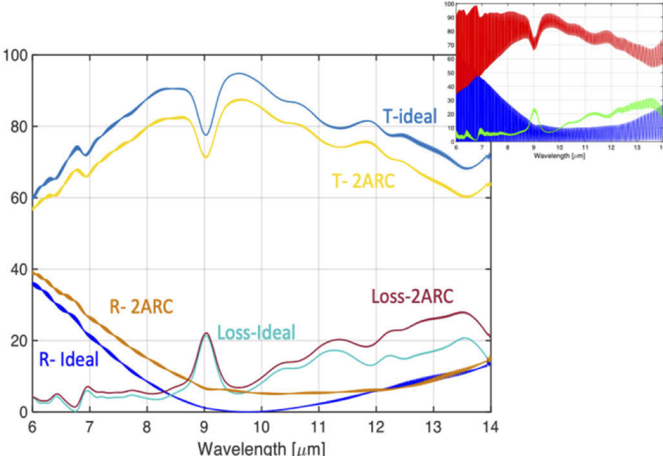

Fig. 10. Simulated transmittance (T), reflectance (R) and loss of a 700 μm thick silicon wafer with an ideal double side quarter wavelength ARC (blue lines) compared with our proposed double ARC (brown lines). Results have been smoothed with a moving average filter of 0.15 μm. In the inset, the unfiltered responses with the evident ripple due to the spurious Fabry Pérot cavity effect.

with respect the single ARC. It should be noted that, despite the addition of a second Al_2O_3 layer, the overall loss of the double ARC (Loss-2ARC, red line) is lower than that of the single ARC, because of the reduced field enhancement in the stack and in particular in the lossy Si layer.

Figure 10 shows the comparison between the ideal quarter wavelength ARC, defined previously, and the proposed solution: the difference in terms of transmittance and reflectance stays below 8% around 10 μm being the loss almost the same in that wavelength region.

The effect of the Al_2O_3 thickness is reported in Fig. 11(a), showing the transmittance (red lines), reflectance (blue lines) and loss (green lines) for d_{Al2O3} values in the range 0 to 100 nm. The black thicker line refers to the case $d_{Al2O3} = 20$ nm. Increasing d_{Al2O3}, the ZnS thickness

Optical Materials EXPRESS

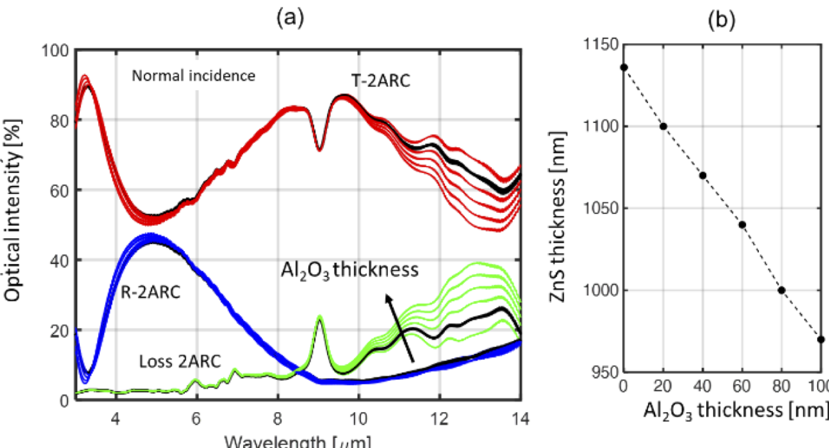

Fig. 11. (a) Double ARC simulated Transmittance T (red), Reflectance R (blue) and Loss (green) for Al_2O_3 thickness from 0 to 100 nm (20 nm step). Black lines refer to $d_{Al2O3} = 20$ nm. (b) Required thickness of the ZnS film to maintain constant the central wavelength of the ARC transmission band versus increasing values of the Al_2O_3 thickness.

must be adapted accordingly in order to maintain the central wavelength of the transmission band [see Fig. 10(b)]. For wavelengths below 10 µm, the loss is dominated by the Si absorption and an Al_2O_3 layer of up to 100 nm introduces a negligible contribution (<3%), with almost no effect on the transmitted power. Above 12 µm, where the Al_2O_3 extinction coefficient is > 1 [see Fig. 7(d)], 100 nm of Al_2O_3 introduces a loss comparable to that of the 700 µm thick wafer resulting in a more than 20% transmission reduction. By using a 20 nm thick Al_2O_3 layer, the additional losses never exceed 4% all across the considered wavelength range. It should be noted that the reflected power (R-2ARC, blue lines) is almost independent from the Al_2O_3 layer thickness (< 4%).

To assess the performance of the ARC on a broad wavelength range (6–20 µm) we evaluated the integral transmission considering as a reference spectrum the radiation of a black body at 36°C. We define the transmission enhancement of the ARC the ratio between the integral transmission

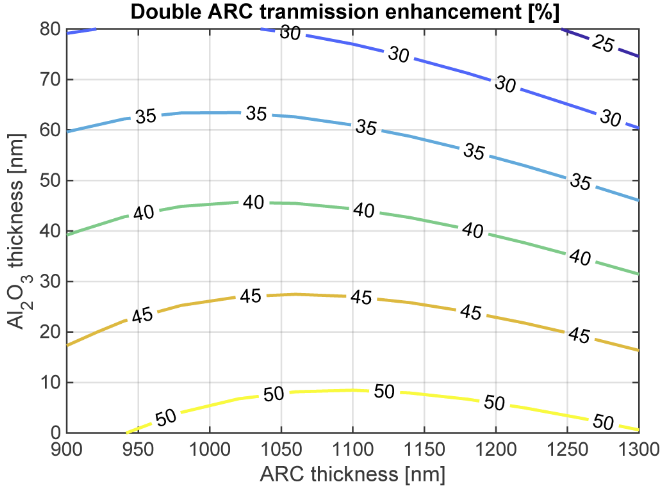

Fig. 12. Double ARC integral transmission enhancement in the range 6 to 20 µm referred to the spectrum of blackbody radiation at 36°C.

Optical Materials EXPRESS

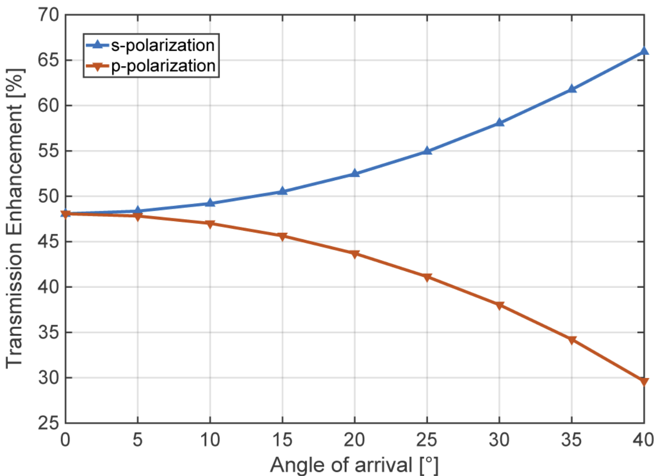

Fig. 13. Simulated double ARC transmission enhancement for *s* and *p* polarization at different angles of incidence.

provided by the ARC for a normally incident black-body radiation with respect to the bare silicon wafer without the ARC. Figure 12 shows in a contour map the transmission enhancement versus increasing thicknesses of the ZnS and Al_2O_3 films. Results shows that the ARC behavior is robust against non-ideal thicknesses of the ZnS film: considering a minimum thickness of 20 nm for the Al_2O_3 adhesion layer, the transmission enhancement remains well above 45% all over ± 200 nm tolerance in the ZnS thickness. On the other hand, 10 nm additional thickness of the Al_2O_3 adhesion layer is responsible for a 4% decrease of the transmission enhancement.

Further, we investigated the sensitivity of the transmission enhancement to the incidence angle of the light radiation for both *s* and *p* polarizations. Figure 13 shows that, when the direction of the light moves from normal incidence to 40°, the transmission enhancement provided by the ARC improves for *s*-polarized light and decreases for *p*-polarized light. Quantitatively, the change of the transmission performance with the incidence angle for the two polarizations balances in such a way that for unpolarized light the transmission enhancement is expected to be almost independent from the incidence angle.

4. Experimental validation

The transmittance characterization of the silicon sample with both single and double ARC was carried out with the spectrometer Frontier FTIR working in the NIR-LWIR wavenumber range from 14.700 - 350 cm^{-1} with a high signal to noise ratio (50.000:1) and a spectral resolution of 4 cm^{-1} [21]. Fabry-Pérot cavity effects are managed by the acquisition conditions.

Figure 14 compares the experimental results of transmittances through a silicon sample 700 µm thick in different conditions: a bare silicon sample (blue), a sample with only a 20-nm-thick layer of Al_2O_3 (green), a sample with a single ZnS ARC of 1136 nm (red), and a sample with a complete single side ARC (yellow). Above 10 µm wavelength the impact of the absorption of the Al_2O_3 layer on the transmission is evident even if limited to a few percent, and it is almost negligible when combined with the ZnS layer because of the lower confinement of the field in the adhesion layer. Below 9 µm the presence of the Al_2O_3 film is even beneficial as contribute to the overall wave matching. Figure 15 presents the comparison between the measured (solid lines) and simulated (dashed lines) transmittance through the sample with the single ARC (red) and double ARC (yellow) with respect to the uncoated silicon sample. The transmittance peak at 10 µm for the double coated wafer is 89% vs 66% for the single coated one, in excellent agreement

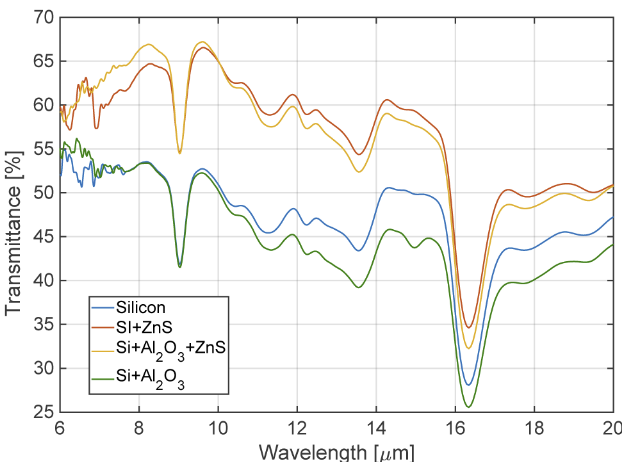

Fig. 14. Measured transmittance of the stack with and without Al_2O_3 adhesion layer.

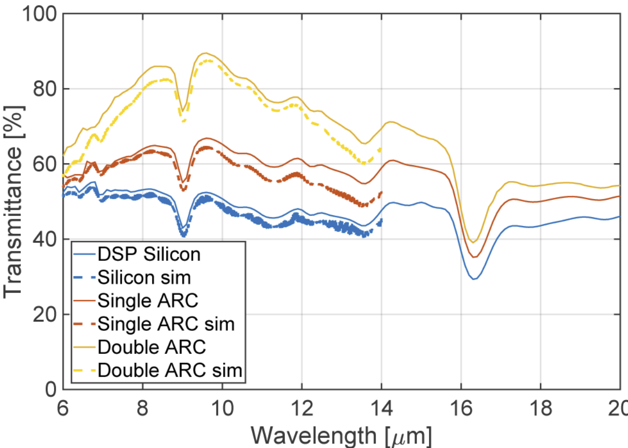

Fig. 15. Comparison of simulated (dashed line) and measured (solid line) transmittance through a silicon sample uncoated (blue), with a single ARC (red) and a double side ARC (yellow).

with simulations. The numerical results extend up to a wavelength of 14 µm as no reliable data on the refractive index n and extinction coefficient k of Al_2O_3 are available at longer wavelengths. Without any ARC, the transmitted power of the 8" silicon wafer is 51.6% integrated on the 3 - 20 µm range. With only a single ARC, the percentage of transmitted power becomes 62.3%, with an improvement of 20.7%. Considering a double ARC, the transmitted power increases to 76.2%, that is 47.7% higher than the bare silicon wafer.

5. Conclusion

The deposition of a ZnS film on silicon and its further characterization have been described in detail, pointing out the main issues related to deposition at room temperature. The proposed solution based on the use of a thin Al_2O_3 interlayer provides good mechanical properties with negligible degradation of the optical transmission. A systematic numerical investigation was carried out to investigate the performance of an ARC operating at 10 µm in terms of

Optical Materials EXPRESS

peak transmittance, robustness versus tolerances of the ZnS layer thickness, wavelength and polarization sensitivity. Despite the non-ideal value of the refractive index of ZnS with respect to an ideal material for a quarter wavelength ARC, experimental results show a peak transmittance of 66% for single-side ARC and 89% for a double-side ARC at a wavelength of 10 µm. The latter structure exhibits an average transmission of 76.2% for black body radiation at 36 °C in the 6–20 µm wavelength range. These results demonstrate the reliability of the simulation tool and the high quality of the ZnS film deposited by using the proposed low-temperature process.

Acknowledgement. The work was mainly performed at Polifab (https://www.polifab.polimi.it/), the micro- and nanofabrication facility of Politecnico di Milano within the Joint Research Centre "MEMS" agreement between Politecnico di Milano and STMicroelectronics.

Disclosures. The authors declare no conflicts of interest.

Data availability. Data underlying the results presented in this paper are not publicly available at this time but may be obtained from the authors upon reasonable request.

References

1. J. Hodgkinson and R. P. Tatam, "Optical gas sensing: a review," Meas. Sci. Technol. **24**(1), 012004 (2013).
2. D. Chandler-Horowitz and P. M. Amirtharaj, "High-accuracy, midinfrared ($450\,cm^{-1} \leq \omega \leq 4000\,cm^{-1}$) refractive index values of silicon," J. Appl. Phys. **97**(12), 123526 (2005).
3. D. C. Harris, *Materials for Infrared Windows and Domes* (SPIE Optical Engineering Press, 1999).
4. M. Gholampour, A. Miri, S. I. Karanian, and A. Mohammadi, "Design and fabrication of multi-layers infrared antireflection nanostructure on ZnS substrate," Acta Phys. Pol. A **136**(3), 527–530 (2019).
5. D. H. Hwang, J. H. Ahn, K. N. Hui, K. S. Hui, and S. Young Guk, "Structural and optical properties of ZnS thin films deposited by RF magnetron sputtering," Nanoscale Res Lett **7**(1), 26 (2012).
6. P. P. Hankare, P. A. Chate, D. J. Sathe, and A. A. Patil, "Structure, surface morphological and opto-electronic properties of zinc sulphide thin films deposited by dip method," Appl. Surf. Sci. **256**(1), 81–84 (2009).
7. P. Offor, B. A. Okorie, F. Ezema, V. S. Aigbodion, C. C. Daniel-Mkpume, and A. Omah, "Synthesis and characterization of nanocrystalline zinc sulphide thin films by chemical spray pyrolysis," Journal of Alloys and Compounds. **650**, 381–385 (2015).
8. M. Ismail Fathima and K. S. Joseph Wilson, "Antireflection coating application of zinc sulfide thin films by nebulizer spray pyrolysis technique," AIP Conf. Proc. **2115**, 030327 (2019).
9. M. Yokoyama, K. Kashiro, and S. Ohta, "Substrate temperature effect on crystallographic quality and surface morphology of zinc sulfide films on (100)-oriented silicon substrates by molecular-beam epitaxy," J. Appl. Phys. **60**(10), 3508–3511 (1986).
10. M. B. Kala, P. K. Bandyopadhyay, and B. B. Nautiyal, "Thorium free antireflection coating in MWIR region on silicon optics," Infrared Phys. Technol. **55**(5), 409–411 (2012).
11. A. Behranvand, M. Davoudi Darareh, M. Jannesari, and M. Mahdavi, "Design and fabrication of PbTe/BaF_2 hydrophobic high-efficiency broad-band antireflection coating on Ge substrate in long-wave infrared region," Infrared Phys. Technol. **92**, 163–165 (2018).
12. G. G. Stoney, "The tension of metallic films deposited by electrolysis," Proc. R. Soc. Lond. A **82**(553), 172–175 (1909).
13. Mil-F-48616, U.S. Department of Defense (1977), (section 4.6.8.1).
14. F. Habel and V. Pervak, "Dispersive mirror for the mid-infrared spectral range of 9–11.5 µm," Appl. Opt. **56**(4), C71–C74 (2017).
15. M. Sánchez-Agudo, I. Génova, H. Orr, G. Harris, and G. Perez, "ZnS films for infrared optical coatings: Improvement of adhesion to Ge substrates," Proceedings of SPIE - The International Society for Optical Engineering. **7101**, 71011K (2008).
16. T. Amotchkina, M. Trubetskov, D. Hahner, and V. Pervak, "Characterization of e-beam evaporated Ge, YbF_3, ZnS, and LaF_3 thin films for laser-oriented coatings," Appl. Opt. **59**(5), A40–A47 (2020).
17. M. R. Querry. "Optical constants of minerals and other materials from the millimeter to the ultraviolet," Contractor Report CRDEC-CR-88009 (1987).
18. J. Kischkat, "Mid-infrared optical properties of thin films of aluminium oxide, titanium dioxide, silicon dioxide, aluminium nitride, and silicon nitride," Appl. Opt. **51**(28), 6789–6798 (2012).
19. C. C. Katsidis and D. I. Siapkas, "General transfer-matrix method for optical multilayer systems with coherent, partially coherent, and incoherent interference," Appl. Opt. **41**(19), 3978–3987 (2002).
20. R. C. Newman, "Oxygen diffusion and precipitation in Czochralski silicon," J. Phys.: Condens. Matter **12**(25), R335–R365 (2000).
21. https://www.perkinelmer.com/it/Product/spectrum-3-nir-mir-reflectance-analyzer-l1280085